Bioactive Materials 6 (2021) 4592–4606

Contents lists available at ScienceDirect

Bioactive Materials

journal homepage: www.sciencedirect.com/journal/bioactive-materials

An intrinsically bioactive hydrogel with on-demand drug release behaviors for diabetic wound healing

Bin Hu [a], Mingzhu Gao [a], Kofi Oti Boakye-Yiadom [a], William Ho [b], Wei Yu [a], Xiaoyang Xu [b,**], Xue-Qing Zhang [a,*]

[a] Engineering Research Center of Cell & Therapeutic Antibody, Ministry of Education, and School of Pharmacy, Shanghai Jiao Tong University, 800 Dongchuan Road, Shanghai, 200240, PR China

[b] Department of Chemical and Materials Engineering, New Jersey Institute of Technology, Newark, NJ, 07102, USA

ARTICLE INFO

Keywords:
Bioactive hydrogel
Drug delivery
Anti-Inflammation
Antioxidant
Diabetic wound healing

ABSTRACT

Prolonged, intense inflammation and excessive oxidative stress hinder diabetic wounds from healing normally, leading to disorders downstream including the postponement of re-epithelialization and extracellular matrix (ECM) formation. Herein, we report a hyaluronic acid (HA) and chitosan based hydrogel (OHA-CMC) with inherent antibacterial and hemostatic activities fabricated via Schiff base reaction. By encapsulating nanotechnologically-modified curcumin (CNP) and epidermal growth factor (EGF) into the hydrogel, OHA-CMC/CNP/EGF exhibited extraordinary antioxidant, anti-inflammatory, and migration-promoting effects in vitro. Meanwhile, OHA-CMC/CNP/EGF presented on-demand drug release in synchrony with the phases of the wound healing process. Specifically, curcumin was rapidly and constantly released to alleviate inflammation and oxidative stress in the early phase of wound healing, while a more gradual and sustained release of EGF supported late proliferation and ECM remodeling. In a diabetic full-thickness skin defect model, OHA-CMC/CNP/EGF dramatically improved wound healing with ideal re-epithelialization, granulation tissue formation, and skin appendage regeneration, highlighting the enormous therapeutic potential this biomaterial holds as a diabetic wound dressing.

1. Introduction

Chronic non-healing diabetic wounds are the major long-term complication of diabetes as their presence significantly increases the chances of clinical infection and amputation. This poses an enormous burden to the healthcare system [1,2]. The skin regeneration from normal wounds undergoes mainly four overlapping yet distinct phases including hemostasis, inflammation, cell proliferation, and matrix remodeling [3]. However, the healing process of refractory diabetic wounds usually violates this timeline and stalls in certain phases due to perpetual hyperglycemia [4,5]. In particular, an extended and intensified inflammation phase is common as a result of macrophage dysfunction and the infiltration and persistence of neutrophils in the wound bed, causing excessive production of proinflammatory cytokines and proteases as well as the reduction of growth factors [6–8]. The cascade of aberrant inflammatory responses disturbs the behaviors of functional cells, including keratinocytes, fibroblasts, and endothelial cells, and even causes injury and apoptosis to the cells [9,10]. Simultaneously, the inflammatory cells recruited at the wound site produce massive amounts of reactive oxygen species (ROS), which aggravates oxidative stress and results in multiple deleterious effects, including reduced collagen deposition and angiogenesis, inappropriate degradation of ECM and growth factors, and postponed re-epithelialization [6,11]. It is therefore essential to develop effective strategies for the timely resolution of disordered inflammation, elimination of excessive ROS, and replenishment of appropriate growth factors in the wound microenvironment to accelerate diabetic wound healing.

To this end, we propose a hydrogel-mediated combinatorial drug delivery approach that modulates inflammation and oxidative stress, and promotes tissue regeneration for improved diabetic wound treatment. Specifically, a hybrid hydrogel based on HA and chitosan was developed to locally co-deliver curcumin and EGF (illustration of Fig. 1).

Peer review under responsibility of KeAi Communications Co., Ltd.

* Corresponding author.
** Corresponding author.
E-mail addresses: xiaoyang.xu@njit.edu (X. Xu), xueqingzhang@sjtu.edu.cn (X.-Q. Zhang).

https://doi.org/10.1016/j.bioactmat.2021.04.040
Received 9 March 2021; Received in revised form 20 April 2021; Accepted 24 April 2021

This optimized combinatorial approach can provide 1) structural support for the wound cavity using degradable and biocompatible ECM-mimicking materials with tunable physical properties; 2) intrinsic antibacterial and hemostatic abilities for the inhibition of wound infection and constant hemorrhage; and 3) co-delivery of small molecules and biological macromolecules with sequential release that accurately satisfies the repair requirements of each healing stage. This platform is designed to meet complex demands for rebuilding the lesioned tissues. To the best of our knowledge, this is the first attempt to manage diabetic wounds by simultaneously delivering small molecules and biomacromolecules with the hydrogel based on the naturally occurring materials HA and chitosan.

Curcumin is a highly pleiotropic compound with well-documented anti-inflammatory and antioxidant activities. Curcumin effectively prevents the generation of proinflammatory cytokines, including tumor necrosis factor-alpha (TNF-α) and interleukin-1 beta (IL-1β) [12]. By inhibiting the activity of NF-κB, the transcription factor that initiates downstream inflammatory responses, and kinases activating PI3K/AKT/NF-κB pathway, curcumin has potent modulatory effects on inflammation [12]. Curcumin also possesses a remarkable ability to scavenge ROS and enhance the activities of antioxidant enzymes [13]. However, the therapeutic feasibility of curcumin is still challenging due to its poor hydrophilicity and bioavailability, short half-life, and chemical instability [14]. Notably, a high dosage of curcumin induces endoplasmic reticulum stress, leading to mitochondrial compartment destabilization and cell apoptosis [15]. On the other hand, EGF plays a vital role in dermal regeneration by stimulating cell proliferation and migration, and the formation of granulation tissue and ECM [16]. However, topical administration of soluble EGF generates rapid delocalization in moisturized wound regions and degradation by the proteolytic microenvironment [17,18]. To address this issue, active EGF was loaded into patches, scaffolds, and hydrogel matrix to maintain the appropriate concentration in the wound bed [19–21]. Although the use of EGF promoted angiogenesis and ECM formation, its ability to modulate the disordered inflammation phase has been rarely reported. Recently, various types of nanoparticles, bandages, and composite systems have been developed as carriers to co-deliver curcumin and EGF for wound healing [22–24]. However, few works reported the precise manipulation of the release of curcumin and EGF as well as the impact of the controlled release pattern on each wound healing phase.

In recent years, research has focused on hydrogels as wound dressings. Benefiting from natural three-dimensional hydrophilic networks, hydrogels offer a moist and occlusive microenvironment and promote the penetration of oxygen and nutrients that support tissue regeneration [25–27]. A variety of payloads, including small molecules, proteins, and living cells, can be loaded into the hydrogel matrix, protected from denaturation or degradation, and released in a controlled manner [28–31]. As a natural polysaccharide with excellent gelation properties, biocompatibility, and water retention capacity, HA has been reported to promote angiogenesis and dermal regeneration, which presents tremendous potential as a wound dressing material [32,33]. Chitosan is extensively associated with the treatment of wounds due to its non-antigenic, antimicrobial, tissue-adhesive, and hemostatic properties [34], which has culminated in its utilization as a commercial wound dressing.

In this study, aldehyde HA (OHA) and carboxymethyl chitosan (CMC) were synthesized and crosslinked via Schiff base reaction to yield hydrogels, whose mechanical properties, biocompatibility, hemostatic ability, and antibacterial activity were well verified. To regulate the undesirable physicochemical characteristics of curcumin, it was encapsulated into polymeric nanoparticles, and then loaded into OHA-CMC together with EGF. In vitro studies showed the extraordinary abilities of OHA-CMC/CNP/EGF to scavenge ROS, attenuate inflammation, and promote cell migration. Moreover, curcumin and EGF were released in

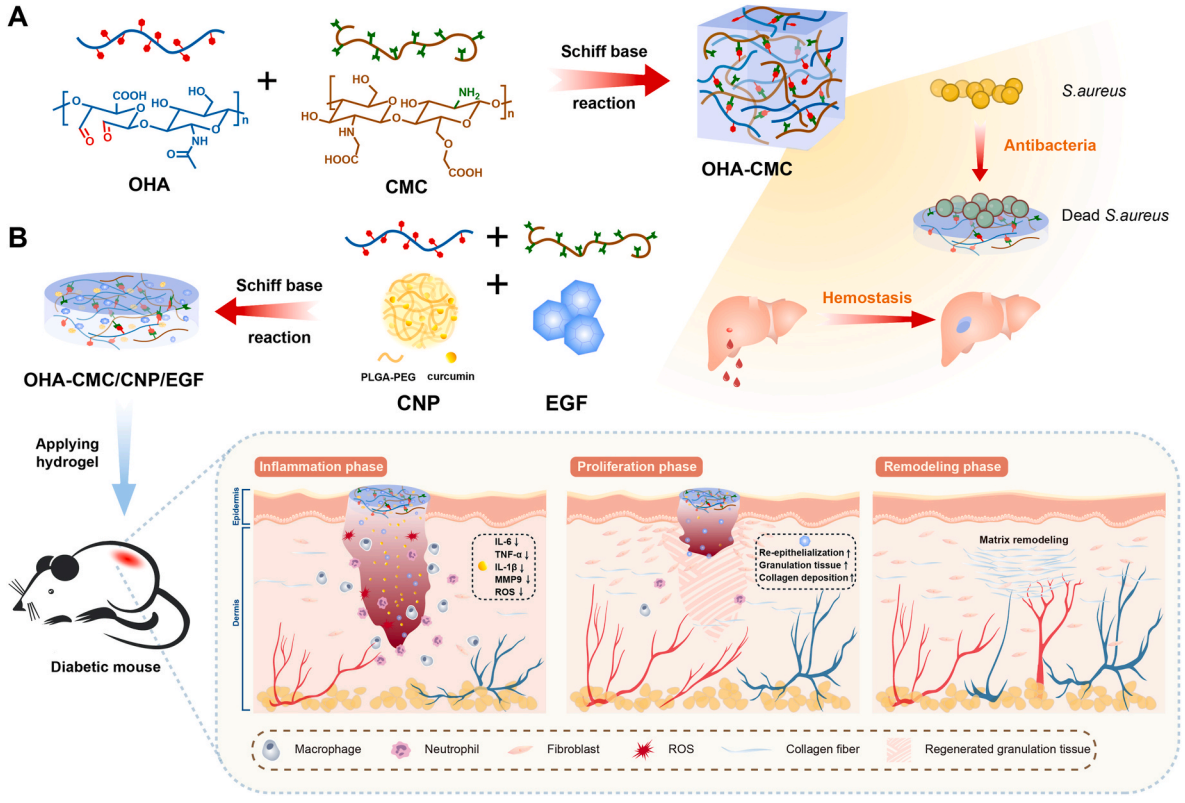

Fig. 1. Schematic representations of OHA-CMC/CNP/EGF hydrogel for diabetic wound healing. (A) OHA-CMC hydrogel was fabricated via reversible Schiff base reaction between OHA and CMC and presented excellent intrinsic antibacterial and hemostatic properties. (B) OHA-CMC/CNP/EGF released drugs in a stepwise manner to solve the key issues in different phases of diabetic wound healing.

sequence due to the significant differences in their physicochemical properties and dynamic chemical bonds between EGF and the hydrogel network, which perfectly synchronized with the diabetic wound healing process. Specifically, curcumin was rapidly released to timely suppress early inflammation and oxidative stress in diabetic wounds, while EGF was released more gradually to support late proliferation and ECM formation. Thus, these two drugs exerted a synergistic therapeutic effect on a full-thickness skin defect model of diabetic mice. In short, the present study proposes a novel strategy for the co-delivery of small molecules and growth factors using a hydrogel with intrinsic bioactivity. We hypothesize that the synergistic effects of curcumin and EGF, combined with regulated drug release by OHA-CMC hydrogel to provide desired concentrations of the corresponding drug locally in specific wound healing phases, can greatly enhance the treatment of diabetic wounds.

2. Materials and methods

2.1. Materials

HA (Mw = 100 kDa) was purchased from Bloomage Freda Biopharm Co., Ltd. (China). HA (Mw = 40 kDa–1000 kDa) was purchased from Shanghai Yuanye Bio-Technology Co., Ltd. (China). Chitosan was obtained from Shanghai Aladdin Bio-Chem Technology Co., Ltd. (China). Curcumin was obtained from Tianjin Guangfu Fine Chemical Research Institute (China). EGF was purchased from PeproTech (USA). Dulbecco's modified Eagle's medium (DMEM), fetal bovine serum (FBS), Trypsin-EDTA, and Penicillin-Streptomycin solution were purchased from Gibco (USA). Unmentioned agents were purchased from Sigma-Aldrich (USA) unless otherwise indicated.

2.2. Synthesis of OHA

OHA was synthesized according to a previous work with slight modifications [35]. Briefly, 0.5 g (~1.25 mmol) HA of different molecular weights were respectively dissolved in 50 mL double distilled water (ddH_2O). 0.1069 g (0.5 mmol) and 0.2674 g (1.25 mmol) $NaIO_4$ were then prepared into 5 ml aqueous solutions and added dropwise to different HA solutions, respectively. The reactions were allowed to proceed at ambient temperature in the dark for 2 h. 0.5 mL ethylene glycol was added to each reaction to quench unreacted $NaIO_4$ and the reactions were stirred for another 1 h. The products were purified through exhaustive dialysis (MWCO 3000) against ddH_2O for three days followed by lyophilization. The yielded OHAs were respectively referred to as LL (Mw = 100 kDa, the molar ratio of HA to $NaIO_4$ (MR) = 5:2), LH (Mw = 100 kDa, MR = 5:5), HL (Mw = 400–1000 kDa, MR = 5:2), and HH (Mw = 400–1000 kDa, MR = 5:5) in the following studies. The degree of oxidation was confirmed using a hydroxylamine titration method [36]. The degree of oxidation of LL, LH, HL, and HH was determined as 27.9%, 56.0%, 33.5%, and 52.7%, respectively.

2.3. Synthesis of CMC

CMC was synthesized according to previous work with slight modifications [37]. 2 g chitosan was dispersed in 10 mL 50% NaOH solution and kept at −20 °C overnight. The thawed alkaline chitosan was then transferred to a round-bottom flask containing 10 mL isopropanol. The mixture was stirred vigorously. Next, 5.7 g chloroacetic acid in 10 mL isopropanol was added dropwise within 30 min and allowed for continuous stirring for another 1.5 h. Then the reaction proceeded at 60 °C for 2 h followed by filtration. The solid product was collected and thoroughly rinsed with 70% (v/v) ethanol/water solution and ethanol. After drying at ambient temperature, the crude product was dissolved in ddH_2O and neutralized with 6 M HCl. The insoluble substance was discarded by centrifugation at 5000*g* for 10 min. CMC was finally obtained by exhaustive dialysis (MWCO 3000) against ddH_2O for 5 days and lyophilization.

2.4. Preparation of hydrogels and drug-loaded hydrogels

OHAs were dissolved in phosphate buffer saline (PBS) (10 mM, pH 7.4) to final concentrations of 1% (w/v), 2% (w/v), and 3% (w/v). CMC was dissolved in PBS to final concentrations of 1% (w/v), 2% (w/v), 3% (w/v), and 4% (w/v). An equal volume of OHA and CMC solution was mixed homogenously and kept at 37 °C for complete hydrogel formation. The obtained hydrogels were named according to the concentrations of the precursor solutions. For example, the hydrogel prepared with 3% HH and 4% CMC was named HH3CMC4. To encapsulate curcumin and EGF into the hydrogel, CNP and EGF aqueous solution containing the desired amounts of drugs were mixed with CMC solution and then formed hydrogel with OHA.

2.5. Characterizations of hydrogels

The gelation time of hydrogels was determined using a vial inverting method. Briefly, the precursor solutions were added to vials and allowed for gelation at 37 °C. The fluidity of the mixture was observed and the gelation time was determined when the samples stopped flowing upon vial inversion.

The rheological characteristics of hydrogels were tested with a Kinexus ultra+ rheometer (Malvern). Briefly, 500 μL hydrogel was placed between 25-mm parallel plates with a gap of 0.75 mm. The storage modulus (G′) and loss modulus(G″) of hydrogels were analyzed under oscillatory mode. At a constant strain of 1%, the frequency sweep tests were performed at 37 °C.

The swelling behavior of hydrogels was examined. The hydrogels were equilibrated in PBS at 37 °C for 24 h to remove the unreacted sol fraction followed by lyophilization. The weighed dry hydrogels (W_0) were immersed into PBS and incubated for 24 h. The swollen hydrogels were then picked out and precisely weighed after removing residual water by a filter paper (W_t). The equilibrium swelling ratio (ESR) was calculated as W_t/W_0.

For the degradation kinetics, hydrogel bulks were immersed into PBS or PBS containing 50U/mL hyaluronidase and incubated at 37 °C, 100 rpm. At predetermined time intervals, the hydrogel samples were taken out and rinsed thoroughly with ddH_2O followed by lyophilization and determination of dry weights. PBS or PBS containing 50U/mL of hyaluronidase were changed daily to maintain the correct concentrations. The weight loss percentage was calculated according to the following formula:

$$\text{Weight loss}\% = (W_0\text{-}W_t)/W_0 \times 100\%$$

where W_0 and W_t are the weights of original hydrogels and remaining hydrogels, respectively.

To examine the morphology of hydrogels, they were lyophilized and sprayed with gold films using a sputter coater (Q150T ES plus, Quorum). The morphology of hydrogels was observed with a scanning electron microscope (SEM) (Mira 3, Tescan) operating at 5 kv. NIH ImageJ software was applied to measure the pore size of each hydrogel sample.

2.6. In vitro cytocompatibility and cytotoxicity

NIH-3T3 cells were cultured in DMEM supplemented with 10% (v/v) FBS and penicillin (100 U/mL)/streptomycin (100 μg/mL) and grown in an incubator of 37 °C supplemented with 5% CO_2 under fully humidified conditions. To prepare the cell-encapsulated hydrogel, OHA and CMC polymers were dissolved in complete growth medium, and cells were suspended in CMC solution to a concentration of 2×10^5 cell/mL hydrogel. OHA and CMC solutions were loaded into a 24-well plate and mixed through gentle stirring with a pipette for gelation. 400 μL complete growth medium was supplemented to each well and the plate was

placed into a cell incubator. At predetermined time intervals, the viability of cells was evaluated using a live/dead staining kit (Beyotime, Shanghai) according to the manufacturer's protocol.

The cytotoxicity of hydrogels was assessed. Briefly, 50 μL sterilized hydrogels were prepared and incubated with 1 mL DMEM for 48 h. The hydrogel extracts were collected and supplemented with 10% FBS. NIH-3T3 cells were seeded in a 96-well plate and incubated for 24 h. The culture medium was then replaced by hydrogel extracts and cells were cultured for another 48 h. Cell viability was evaluated with Cell Counting Kit-8 (CCK-8) (Beyotime, Shanghai) according to the manufacturer's instructions, where cells cultured with complete growth medium were used as control.

2.7. Antibacterial performance

The antibacterial activities of hydrogels were tested against *Staphylococcus aureus* (*S. aureus*) (ATCC 25923). Briefly, a total volume of 100 μL hydrogel precursor solutions were loaded into a 96-well plate and kept at 37 °C. The bacterial suspension (10 μl, 10^6 CFU/ml) was then added onto the hydrogel surface and incubated for 6 h. The group of bacteria incubated with 100 μl PBS was set as control. Thereafter, 100 μl PBS was used to resuspend the bacteria, which was subsequently seeded on a nutrient broth plate and cultured overnight. The number of colonies on the plate was counted with ImageJ software.

2.8. Hemostatic ability

A mouse liver bleeding model was used to evaluate the hemostatic ability of the hydrogel. All animal experiments were conducted under the approval of the Animal Care and Use Committee of Shanghai Jiao Tong University. Briefly, the mice were anesthetized followed by liver exposure from an abdominal incision, and filter papers were used to carefully remove the tissue fluid around the lesion. The livers were placed on a pre-weighed filter paper (W_0) and punctured with an 18G needle for bleeding. The commercial hemostatic sponge Merocel, OHA-CMC hydrogel, and lyophilized OHA-CMC were immediately placed onto the bleeding site once upon puncture. The wound without treatment was set as the control. Each group contained five mice. The hemorrhaging site was photographed at 0 s, 15 s, 30 s, and 60 s. The weight of the filter paper at 60s after puncture was measured (W_t). The blood loss was calculated as the weight increase of the filter paper (W_t-W_0).

2.9. In vitro drug release assay

100 μl OHA-CMC hydrogel loaded with CNP (containing 100 μg curcumin) were immersed into 3 mL PBS containing 0.5% (v/v) Tween 20 (pH = 7.4) and placed into a shaking incubator of 37 °C, 100 rpm. At predetermined intervals, 1 mL release medium was withdrawn and 1 mL fresh buffer was supplemented. The absorbance of release medium at 423 nm was measured. The release amount of curcumin was calculated using a predetermined calibration profile. The in vitro release of EGF from hydrogel was performed in PBS using the aforementioned method. The release amount was quantified with a human EGF ELISA kit (QuantiCyto®, Neobioscience).

2.10. Antioxidant effects of OHA-CMC/CNP hydrogel

The antioxidant capacity of OHA-CMC/CNP hydrogel was evaluated using a 1, 1-diphenyl-2-picrylhydrazyl (DPPH) scavenge assay according to a reported protocol with slight modifications [38]. Briefly, OHA-CMC hydrogels containing different doses of CNP were respectively doped in 1 mM HCl and prepared into homogenate using a tissue grinder. 100 μl hydrogel dispersion was mixed thoroughly with 1 mL 200 μM DPPH solution and incubated in dark for 30 min. The mixture was centrifuged and the absorbance of the supernatant at 517 nm was measured. The DPPH scavenging percentage was calculated using the following equation:

$$\text{DPPH scavenging } (\%) = (A_d\text{-}A_h)/A_d \times 100\%$$

where A_d and A_h represent the absorbance of DPPH solution and hydrogel-treated DPPH solution, respectively.

The intracellular ROS scavenging capacity of OHA-CMC/CNP hydrogel was tested on NIH-3T3 cells. Briefly, cells were seeded in a 24-well plate and cultured for 24 h. The cells were then incubated with hydrogels encapsulated with different doses of CNP and H_2O_2 (650 μM) for another 24 h. After rinsing with PBS, cells were incubated with DCFH-DA (10 μM in FBS-free DMEM) for 20 min. The intracellular ROS level was evaluated by flow cytometry (LSRFortessa™ Flow Cytometer, BD biosciences). Meanwhile, the fluorescence in cells was photographed by a confocal fluorescence microscope (IX73, Olympus).

2.11. In vitro anti-inflammatory efficiency of OHA-CMC/CNP hydrogel

RAW 264.7 cells were seeded on a 24-well plate and cultured overnight. The cell culture medium was replaced by the complete growth medium supplemented with 500 ng/mL lipopolysaccharide (LPS). After incubating for 4 h, cells were rinsed and incubated with hydrogels containing different doses of CNP for 24 h. RNA of the cells was isolated with Trizol and performed with reverse transcription and real-time polymerase chain reaction (RT-PCR). The $2^{-\Delta\Delta CT}$ method was used for TNF-α, IL-1β, and IL-6 mRNA expression analysis. GAPDH was used as the reference gene.

2.12. Scratch wound assay

NIH-3T3 cells were seeded in a 6-well plate and allowed to form a confluent monolayer. The cells were scratched with a sterilized 200 μL pipette tip to form an incisional wound and washed with PBS to remove cell debris. The cells were then cultured with OHA-CMC, OHA-CMC/CNP, OHA-CMC/EGF, and OHA-CMC/CNP/EGF in DMEM supplemented with 2% FBS. The wound sites were photographed and the wound area was calculated with ImageJ software at the time when the wounds were created (A_0) and cells were incubated for 12 h and 24 h (A_t). The wound area (%) was calculated as $A_t/A_0 \times 100\%$.

2.13. In vivo diabetic wound healing performance

The male C57BL/6 mice (6–8 weeks) were intraperitoneally injected with streptozotocin (STZ) (50 mg/kg) for 5 consecutive days after an overnight fast. The blood glucose was measured using a glucose meter (GA-3, Sinocare) after 2 weeks. The mice were considered diabetic when non-fasted blood glucose levels consistently exceeded 16.7 mM. The diabetic mice were anesthetized and shaved with dorsal hair. A full-thickness cutaneous wound with the diameter of 8 mm was created on each mouse using a punch biopsy. The mice were randomly assigned to five groups with different treatments, namely, control, OHA-CMC, OHA-CMC/CNP, OHA-CMC/EGF, and OHA-CMC/CNP/EGF, each of which contained 15 mice. The mice were sacrificed and the wound tissues were collected at predetermined time points. Meanwhile, the wound area was photographed and measured using ImageJ software.

2.14. Histological evaluation

The wound tissues were fixed with 4% paraformaldehyde, embedded in paraffin, and cross sectioned to 5 μm thick slices. The slices were mounted on slides for Haematoxylin-Eosin (H&E) and Masson's trichrome staining according to the manufacturer's instructions. For immunofluorescent and immumohistochemical staining, the slides were stained respectively with Anti-IL-6 antibody (Servicebio, China), Anti-MMP9 antibody (Servicebio, China), Anti-Collagen I antibody

(Servicebio, China), and Anti-CD31 antibody (Servicebio, China) under a standard protocol. Fresh tissues were embedded in optimal cutting temperature and froze and then sectioned to 10 μm thick slices. The slides were stained with dihydroethidium (DHE) (5 μM) to indicate intracellular ROS levels. The stained slides were photographed using a confocal laser microscope (TCS SP8, Leica).

2.15. Statistical analysis

All data from at least three independent experiments were presented as mean ± standard deviation. The differences between groups were analyzed using unpaired two-tailed Student's t-test with GraphPad Prism 8 software. In all cases, the differences were regarded as statistically significant with $^{*}p < 0.05$, $^{**}p < 0.01$, $^{***}p < 0.001$, and $^{****}p < 0.0001$.

3. Results and discussion

3.1. Formation and characterizations of hydrogels

The schematic illustration for the formation of OHA-CMC hydrogel is shown in Fig. 1A. The oxidized HA was obtained by a ring-opening reaction using sodium periodate, which resulted in the introduction of the dialdehyde group into the HA dimer unit (Fig. S1A). Compared to the ^{1}H NMR spectra of HA, two newly-formed peaks at 4.8 ppm and 4.9 ppm were observed on that of OHA, corresponding to the hemiacetal protons and vicinal hydroxyl groups (Fig. S1A). The peak at 1726 cm^{-1} in the Fourier transform infrared (FT-IR) spectra of OHA was the stretching vibration of –C═O– bond of the aldehyde group (Fig. 2A). To increase the aqueous solubility of chitosan, CMC was synthesized and the structure was identified by ^{1}H NMR and FT-IR. The chemical shifts at 3.0 ppm and 4.2 ppm in ^{1}H NMR spectra indicated the protons of –CH_2COO– introduced to amino groups and hydroxyl groups of chitosan, respectively (Fig. S1B). The antisymmetric stretching vibrations and stretching vibration of the carboxylate band of –COO– were reflected as the peaks at 1617 cm^{-1} and 1409 cm^{-1} in the FT-IR spectra of CMC, indicating the successful introduction of carboxymethyl groups into the chitosan polymeric chain (Fig. 2A).

The OHA and CMC polymers formed hydrogels via the Schiff base reaction between the aldehyde groups in OHA and the amino groups in CMC, resulting in the peak at 858 cm^{-1} in the FT-IR spectra of the hydrogel (Fig. 2A). To optimize the gelation conditions, OHAs of different molecular weights and degrees of oxidation (namely, LL, LH, HL, and HH) were synthesized, and different concentrations of OHA and CMC precursors were prepared for gelation. The gelation time was determined using a vial inverting method (Fig. S2A). The hydrogels were formed using all types of OHA with a wide range of gelation concentrations of precursor solutions (Fig. S2B), indicating a high gelation activity of these two polymers. Generally, OHAs with a higher degree of oxidation formed hydrogel with CMC in a more rapid manner (Fig. S2B). The gelation time reduced significantly with an increase in precursor concentrations due to the enhancement of crosslinking density. Especially, LH3CMC4, HH3CMC3, and HH3CMC4 formed within 45 s once the precursors were mixed. The rapid gelation was essential for hydrogel wound dressings which promised immediate occlusion of the wound region and the inhibition of constant hemorrhage and infection once applied [39]. Therefore, LH3CMC4, HH3CMC3, and HH3CMC4 were chosen for subsequent studies.

The rheological properties of the hydrogels were explored to evaluate their mechanical behaviors. The frequency sweep profiles showed that the hydrogels of the indicated compositions had a stable G′ approximately 10 times larger than the G″ in the range of 0.1–10 Hz (Fig. 2B). LH3CMC4 and HH3CMC4 had similar G′ values of about 240 Pa, which was higher than the G′ of HH3CMC3 (146 Pa), suggesting a stronger crosslinked network within LH3CMC4 and HH3CMC4 than HH3CMC3. This was likely due to a relatively low level of reactive amino groups in HH3CMC3, resulting in a lower crosslink density. However, the molecular weight of HA seemed to have little effect on the compactness of the hydrogel structure, which depended mainly on the number of reactive groups.

The swelling behavior of the hydrogels was investigated by incubating in PBS at 37 °C for 24 h. As shown in Fig. 2C, all the hydrogels swelled sharply (ESR from 48 to 58 g/g), which indicated that the hydrogels had the capacity to absorb excessive wound exudates and also

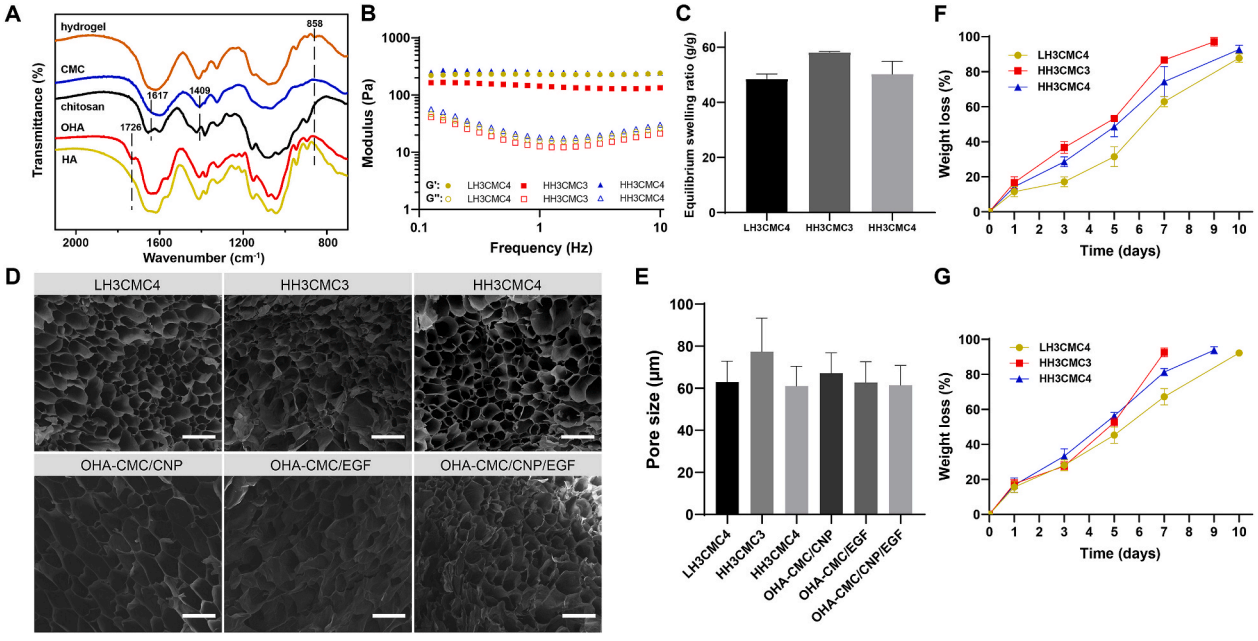

Fig. 2. Characterizations of hydrogels. (A) FT-IR spectra of HA, OHA, chitosan, CMC, and representative hydrogel formed through the Schiff base reaction between OHA and CMC. (B) Rheological behavior of hydrogels. (C) ESR of hydrogels after immersing in PBS for 24 h. (D) Representative SEM images of hydrogels and drug-encapsulated hydrogels. Scale bar: 100 μm. (E) Pore size of hydrogels and drug-encapsulated hydrogels. (F, G) Degradation kinetics of hydrogels in PBS without (F) and with (G) 50 U/mL hyaluronidase.

maintain a moist environment at the wound sites. Meanwhile, the swelling ability of the hydrogels was a reflection of the overall crosslink density, where a higher ESR indicated a weaker crosslinked network [40]. Among the three hydrogels tested, HH3CMC3 was of the highest ESR while LH3CMC4 and HH3CMC4 were of similarly lower ESR, which was consistent with the rheological results.

The morphology of lyophilized hydrogels was observed using SEM. All hydrogels presented a typical interconnected and porous microstructure with uniformly arranged pores (Fig. 2D), intended for efficient transport and permeation of oxygen and nutrients as well as for the exchange of wound waste. The pore size of the hydrogel was largely related to the crosslink density of the hydrogel network. The average pore sizes of LH3CMC4, HH3CMC3, and HH3CMC4 were 62.9 μm, 77.3 μm, and 61.1 μm, respectively (Fig. 2E), revealing a denser interior structure of LH3CMC4 and HH3CMC4 compared to that of HH3CMC3.

In vitro degradation behaviors of the hydrogel samples were evaluated. The degradation of hydrogels was mainly mediated by surface erosion and bulk degradation [41]. As shown in Fig. 2F, LH3CMC4, and HH3CMC4 maintained bulk hydrogel for 10 days with the remaining weight percentage being 12.2% and 7.3% at the end of the investigation period, respectively. However, HH3CMC3 decomposed completely when the degradation proceeded to the 9th day, owing to its less crosslinked interior networks. The degradation performance in the presence of 50 U/mL of hyaluronidase was also assessed (Fig. 2G). The enzyme-mediated degradation periods of LH3CMC4, HH3CMC3 and HH3CMC4 lasted 10, 7, and 9 days respectively, revealing very slight acceleration compared to degradation kinetics in PBS. This was mainly because hyaluronidase cleaved the β-(1,4) glycosidic linkages of HA and preserved the integrity of HA dimer units, which were still covalently bound to the hydrogel structure. In general, the hydrogels of different formulations were biodegradable and provided a desirable degradation rate for wound healing applications.

3.2. *In vitro cytocompatibility, hemocompatibility, antibacterial ability, and hemostatic ability of hydrogels*

The favorable biocompatibility of a hydrogel is a prerequisite for biomedical applications. In this regard, the cytocompatibility of the hydrogels was studied by encapsulating NIH-3T3 cells into hydrogels, and analyzing cell viability and proliferation with live/dead staining. The number of cells encapsulated in three tested hydrogels had apparently increased at day 3 and day 7 compared to day 1 (Fig. 3A), showing

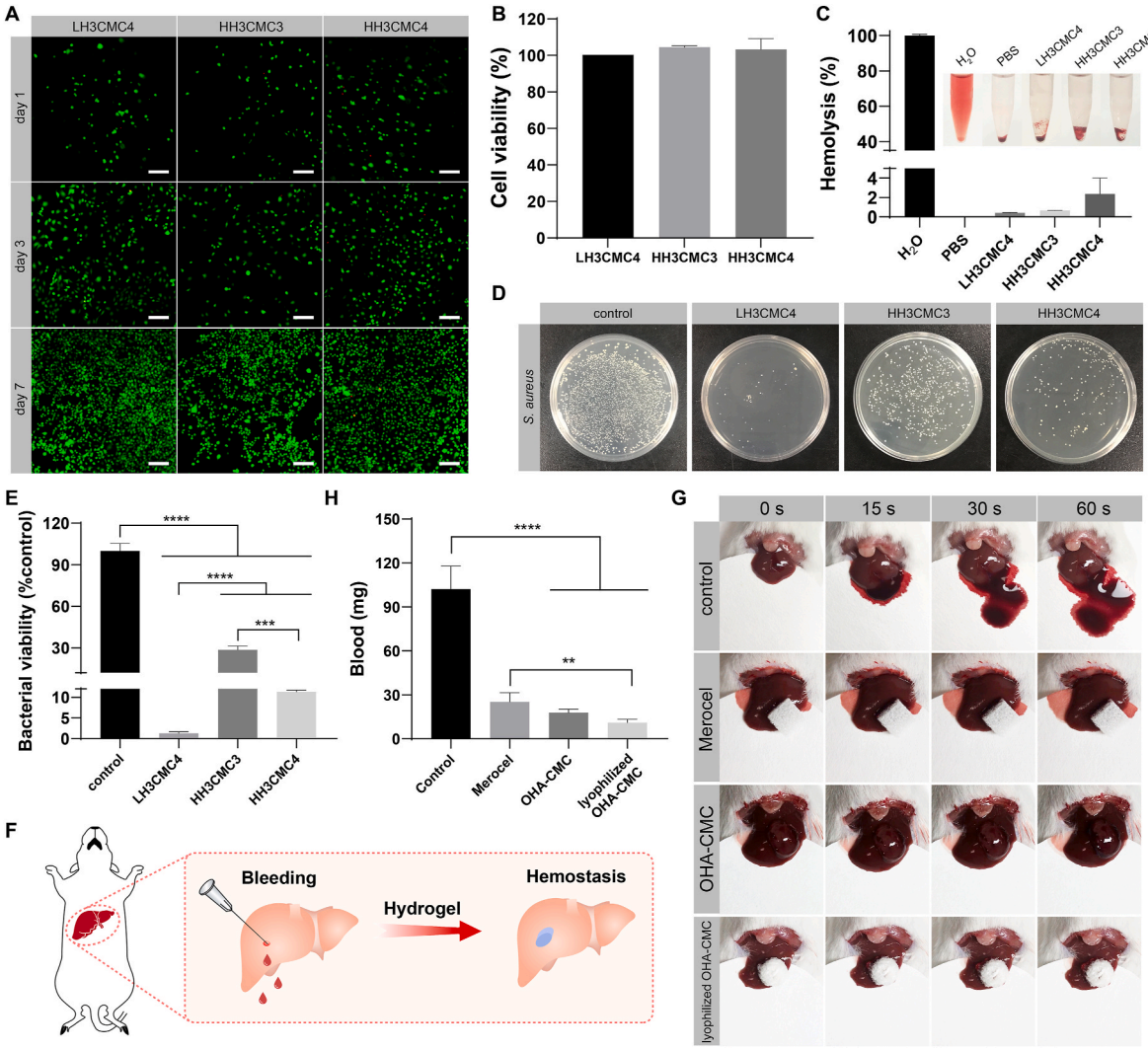

Fig. 3. (A) Cytocompatibility of hydrogels indicated by live/dead staining. Scale bar: 200 μm. (B) Cell viability of NIH-3T3 following incubating with hydrogel extracts for 48 h. (C) Hemolytic ratio of hydrogels. (D, E) Antibacterial analysis of hydrogels. Digital photographs of *S. aureus* colonies (D) and bacterial viability (E) after incubating with hydrogels for 6 h. (F) Schematic diagram illustrating the assessment of the hemostatic performance for the hydrogel via a mouse liver bleeding model. (G) Representative photographs of bleeding livers following different treatments at predetermined time points. (H) Total mass of blood loss in 60s from punctured livers after different treatments.

that all hydrogels commendably supported the growth and proliferation of cells. Few dead cells were observed in the visual field, revealing the desirable cytocompatibility of the hydrogels. The cytotoxicity of hydrogels was further investigated with a CCK-8 assay. As expected, none of the hydrogel extracts showed cell toxicity, and the cells grew with 100% viability under all conditions after 24 h of incubation (Fig. 3B). Furthermore, LH3CMC4, HH3CMC3, and HH3CMC4 had low hemolysis ratios of 0.41%, 0.66%, and 2.36%, respectively (Fig. 3C), indicating their excellent hemocompatibility. These results promised the feasibility of the hydrogels as candidates for wound dressings.

Bacterial infection is one of the critical causes of delayed wound healing in clinical practice and there is a high demand for antibacterial hydrogels [42]. In this study, the antimicrobial behavior of the developed hydrogels was assessed with *S. aureus* as a model bacterium. Expectedly, the number of bacterial colonies remarkably declined in all hydrogel groups compared to the PBS treatment group (Fig. 3D). LH3CMC4, HH3CMC3, and HH3CMC4 contributed to the bacterial inhibition percentages of 98.7%, 71.4%, and 88.7%, respectively (Fig. 3E). The superior antibacterial activity of the hydrogels was attributed to the inherent properties of chitosan. The highly-charged polycationic structure of chitosan generated intense electrostatic interaction with the negatively charged phospholipid membrane components of bacteria, leading to bacterial death through membrane damage and subsequent leakage of contents [43]. The relatively weaker bacteriostasis of HH3CMC3 was ascribed to its lower chitosan content and the dose-dependent antibacterial effects of chitosan. The highly entangled polymeric chain of HA with high molecular weight reduced the potential for electrostatic material-bacteria interaction, resulting in weaker bacteriostasis in HH3CMC4 compared to LH3CMC4. LH3CMC4 was therefore chosen for the following studies and referred to as OHA-CMC hydrogel based on an overall consideration.

The ideal wound dressing was capable of instantaneous hemostasis once the trauma was formed to prevent excessive blood loss. Therefore, the hemostatic ability of OHA-CMC was examined in a mouse hemorrhaging liver model (Fig. 3F). A pronouncedly high hemorrhage was observed in the control group with a blood loss mass of 102.1 mg (Fig. 3G and H). Such hemorrhage was rapidly controlled after OHA-CMC was applied to the bleeding site and the mass of lost blood decreased by 4.7 times, showing even better effects than that of a commercial hemostatic product (where blood loss decreased by only 3 times). The excellent hemostasis of OHA-CMC can be attributed to the physical blockage of the bleeding defect by the 3D hydrogel network and the adhesion of the hydrogel on the tissue surface [44]. Simultaneously, the positively charged amino groups on the hydrogel interacted with the negatively charged platelets through electrostatic force, which activated the blood coagulation process [45]. Notably, the lyophilized OHA-CMC had the best hemostatic performance with a blood loss of 11.2 mg due to its additional ability to rapidly absorb fluid around the bleeding site compared to OHA-CMC, indicating the enormous potential of the hydrogel for clinical translation.

3.3. Encapsulation of curcumin and EGF in OHA-CMC hydrogel and their in vitro release behaviors

Curcumin and EGF, therapeutic agents for diabetic wounds, were encapsulated into OHA-CMC hydrogel. Since curcumin is highly hydrophobic and chemically unstable, it was loaded into PLGA-PEG nanoparticles to improve its aqueous solubility and stability. PLGA-PEG was synthesized and the structure was verified through ^{1}H NMR (Fig. S3). Different methods and material ratios were tested to optimize the size, polymer dispersity index (PDI), encapsulation efficiency, and drug loading efficiency of CNP (Table S1). The solubility of CNP was significantly enhanced compared to that of free curcumin. Specifically, curcumin remained undissolved in PBS at 100 μg/mL but was able to achieve a concentration of 500 μg/mL in the form of CNP (Fig. S4A). It has been reported that free curcumin induced apoptosis in fibroblasts at concentrations higher than 10 μg/mL [46]. It is noteworthy that CNP showed no cytotoxicity in NIH-3T3 within the curcumin concentration range of 0.1–10 μg/mL (Fig. S4B).

CNP and EGF were loaded into the hydrogel matrix by simple incorporation of the drugs in hydrogel precursors. SEM images indicated that the encapsulation of CNP, EGF, or co-encapsulation of the drugs had no impact on the internal structure of the hydrogel with the pore sizes of 67.1 μm, 62.4 μm, and 61.5 μm, respectively (Fig. 2D and E). The in vitro release behaviors were subsequently studied. There was an obvious burst release of curcumin from OHA-CMC hydrogel, where the cumulative release percentage was up to 55.3% on day 1 and 75.5% on day 3 (Fig. 4A). The release rate was then slowed down and curcumin was continuously released for another three days. EGF showed a relatively slight burst release of 28.6% on day 1 and 51.3% on day 2 followed by a sustained release. About 88.1% of EGF were released in 9 days. The release of the therapeutic agents was mainly mediated by the diffusion and the degradation of the hydrogel backbone. However, EGF possessed significantly slower and more sustained release kinetics compared with curcumin due to its larger molecular structure accompanied with increased steric hindrance during its diffusion from the hydrogel. Moreover, the free amino groups in EGF structure dynamically participated in Schiff base reaction, which led to the covalent binding of EGF to the hydrogel network and further prolonged the release process of EGF. The sequential release of curcumin and EGF were highly advantageous for diabetic wound healing. The abundant release of curcumin in the early phase could timely attenuate inflammation and oxidative stress, while the long-term release of EGF effectively supported cell migration and proliferation and ECM formation in later phases, which perfectly synchronized with the process of wound healing (Fig. 1B).

3.4. Antioxidant and anti-inflammatory abilities of OHA-CMC/CNP hydrogel

Excessive oxidative stress is one of the main causes of delayed diabetic wound healing [47]. Developing hydrogel dressings with ROS scavenging abilities thus becomes a valid strategy for diabetic wound therapy. Herein, curcumin-loaded nanoparticles were encapsulated in the hydrogel and examined for its antioxidative ability, where DPPH was utilized as the modal free radical for detection. As shown in Fig. 4B, DPPH had a strong ultraviolet absorption at 517 nm and the absorbance reduced proportionally after transferring an electron or a hydrogen atom to the odd electron in DPPH• [48]. When treated with OHA-CMC/CNP containing different doses of curcumin in the range of 1–100 μg, DPPH showed a gradual decrease in the intensity of its characteristic peak which disappeared completely with the action of hydrogel containing 25 μg or higher curcumin dosage. OHA-CMC showed almost no DPPH scavenging activity, while hydrogel encapsulating 1 μg, 10 μg, 25 μg, 50 μg, and 100 μg curcumin scavenged 33.6%, 54.9%, 78.9%, 80.3%, and 84.6% of DPPH, respectively (Fig. 4C), demonstrating the remarkable antioxidant activity of OHA-CMC/CNP. To explore the effects of the hydrogel on curcumin, free curcumin solution and OHA-CMC/CNP including the same dose of curcumin were maintained at room temperature and 37 °C for 10 days, during which the antioxidant activities of curcumin from different groups were tested at predetermined time points (Fig. 4D). The DPPH scavenging capacity of curcumin encapsulated in OHA-CMC was almost unchanged and continuously maintained at the initial level whether at room temperature or 37 °C. However, the activity of free curcumin decreased during observation under both conditions. The DPPH scavenging percentage of free curcumin decreased to 62.3% on day 10 at ambient temperature, which showed a more striking decrease to 42.2% when it was placed at 37 °C for 10 days. These results concluded that OHA-CMC hydrogel system exhibited significant protective effects on the antioxidant ability of curcumin, which was because OHA-CMC shielded the direct contact and interaction of curcumin and its surroundings, thereby preventing it from inactivation or degradation by providing a stable environment for

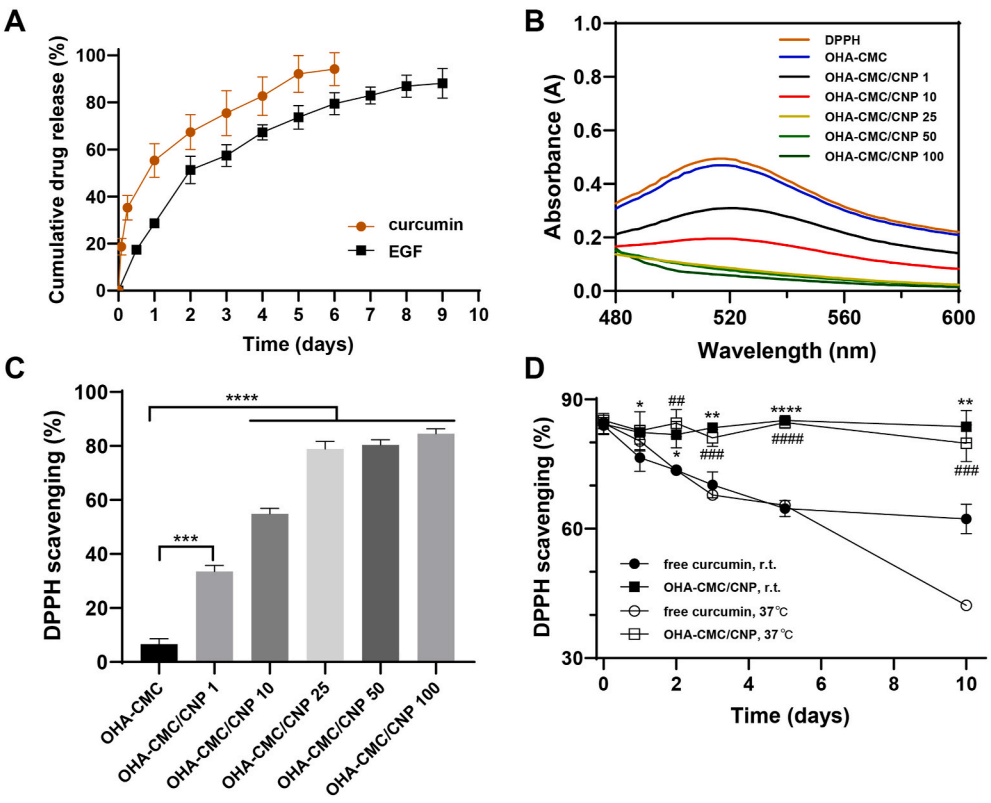

Fig. 4. (A) Drug release profile of curcumin and EGF from OHA-CMC hydrogel. (B) UV–vis spectra of DPPH and DPPH treated with OHA-CMC/CNP containing different doses of curcumin. (C) DPPH scavenging percentage for the treatments with OHA-CMC/CNP containing different doses of curcumin. (D) Changes of DPPH scavenging percentage for free curcumin and OHA-CMC/CNP with the same dose of curcumin kept at room temperature and 37 °C for 10 days. $*p < 0.05$, $**p < 0.01$, and $****p < 0.0001$ comparison between free curcumin and OHA-CMC/CNP at room temperature. $\#\#p < 0.01$, $\#\#\#p < 0.001$, and $\#\#\#\#p < 0.0001$ comparison between free curcumin and OHA-CMC/CNP at 37 °C.

maintaining curcumin activity.

The intracellular ROS scavenging ability of OHA-CMC/CNP was also evaluated using a ROS-specific probe. Fibroblasts were stimulated with H_2O_2 to achieve intracellular oxidative stress and examined on ROS levels following incubation with OHA-CMC or OHA-CMC/CNP, where ROS was labeled with green fluorescence by DCFH-DA. The intensity of green fluorescence was significantly enhanced after H_2O_2 treatment and increased to a level 2.4 times as strong as that of PBS control (Fig. 5A and B). However, when the cells were incubated with OHA-CMC/CNP containing different curcumin doses, a dose-dependent decrease in fluorescence intensity was observed, indicating that OHA-CMC/CNP effectively alleviated the intracellular oxidative stress. In particular, the intracellular ROS level was successfully aligned with the normal level following the treatment of OHA-CMC/CNP containing as low as 1 μg curcumin, suggesting the ability of OHA-CMC/CNP to ameliorate immoderate oxidative stress in the diabetic wound microenvironment.

Inflammation has been recognized as another critical factor hindering diabetic wound healing [49], and effective regulation of inflammatory cytokines is beneficial for the acceleration of diabetic wound healing. In the present study, RAW264.7 cells were stimulated with LPS followed by the treatment of OHA-CMC/CNP, and the intracellular inflammatory cytokine levels including TNF-α, IL-1β, and IL-6 were analyzed using RT-PCR as shown in Fig. 5C. The expression of three examined cytokines was elevated after LPS stimulation as a result of activating cellular inflammatory responses through the canonical NF-κB pathway [50]. Treatment with OHA-CMC showed little impact on levels of inflammatory cytokines. However, all of the cytokine levels were downregulated following the treatment with OHA-CMC/CNP. When various doses of curcumin were administered, the relative mRNA levels decreased in a dose-dependent manner, which were nearly tuned to the initial normal levels after treatment with OHA-CMC/CNP containing a dose of curcumin as low as 5 μg. These results indicated that OHA-CMC/CNP was able to release curcumin and inhibit the expression of inflammatory cytokines in vitro, which is highly desirable in the management of diabetic wounds.

3.5. Migration-promoting effects of OHA-CMC/CNP/EGF hydrogel

Collective cell migration is a hallmark of wound healing and involves a variety of key events during this process, including fibrin clot decomposition, ECM and collagen regeneration, and wound contraction [51], which underlines the need to study the in vitro effects of hydrogels on cell migration. In this study, a scratch wound was created in a monolayer of fibroblasts to evaluate such influences. As evidenced in Fig. 5D and E, the cell migration showed different degrees of enhancement after 12 h and 24 h exposure to various hydrogel formulations. The blank OHA-CMC hydrogel promoted cell migration to a limited extent. When the CNP and EGF were encapsulated into the hydrogel, the remaining percentages of wound area decreased by 10.3% and 21.5% at 12 h and 11.4% and 20.2% at 24 h, respectively, compared to those of the control group. The co-delivery of curcumin and EGF were more potent to accelerate cell migration, contributing to a reduction of 28.6% at 12 h and 25.9% at 24 h on the unclosed wound area percentage, respectively. Curcumin and EGF have been widely reported to facilitate epidermal cell migration in previous studies [46,52], which were further verified in the present study. Additionally, the two therapeutic agents used in combination exhibited synergistic beneficial effects on cell migration with far-reaching potential applications in wound therapy.

3.6. Wound healing performance of hydrogels in a full-thickness cutaneous wound model and histological analysis

The in vivo wound healing performance of the hydrogels was evaluated in a full-thickness cutaneous wound model of diabetic mice (Fig. 6A). A round defect with the diameter of 8 mm was created and treated with different hydrogel formulations. In this study, contraction of local skin was prevented by applying a Tegaderm™ film on the wound so that it healed through granulation and re-epithelialization to better simulate human wound healing [53]. The wound healing was observed and recorded on day 5, 10, and 15 as shown in Fig. 6B and C. On the fifth day after wound formation and hydrogel administration, the control

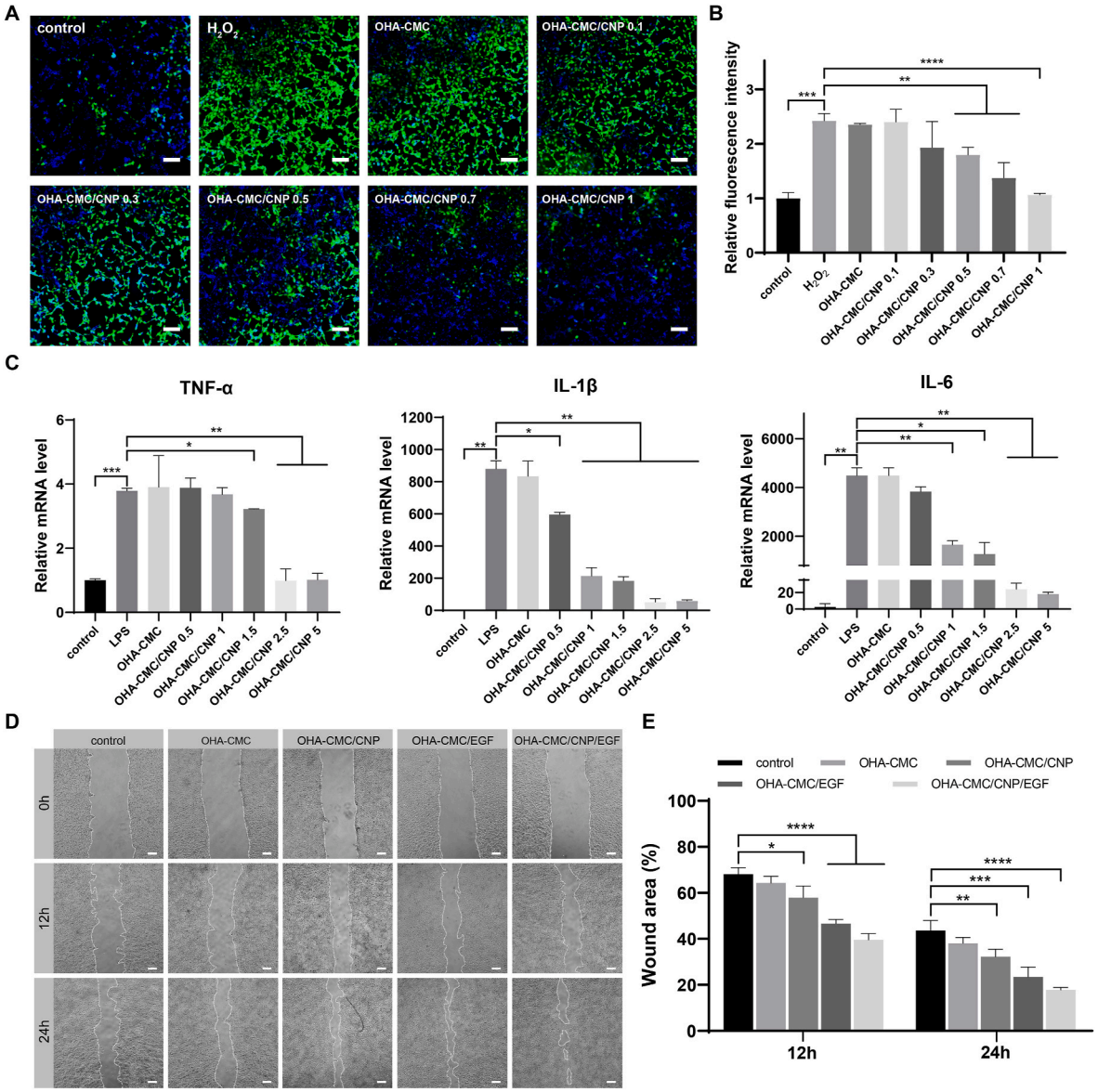

Fig. 5. (A) The intracellular ROS level indicated by DCFH-DA probe following different treatments. Scale bar: 200 μm. (B) The quantitative analysis of intracellular ROS depletion with different treatments by flow cytometry. (C) The RT-PCR analysis of intracellular TNF-α, IL-1β, and IL-6 mRNA level after treatment with OHA-CMC containing different doses of curcumin. (D) Representative photographs of scratch wounds at 0 h, 12 h, and 24 h following the treatments with control, OHA-CMC, OHA-CMC/CNP, OHA-CMC/EGF, and OHA-CMC/CNP/EGF. Scale bar: 200 μm. (E) Quantification of the remaining scratch wound area percentage at 12 h and 24 h with different treatments.

group had the lowest wound closure percentage of 28.2%. The blank OHA-CMC hydrogel presented a weak effect on the promotion of wound healing. However, treatment of CNP- and EGF- encapsulated hydrogels significantly reduced the wound area by the increases of 12.1% and 10.7% in closure percentage relative to that of the control. Notably, OHA-CMC/CNP/EGF had the best therapeutic effects, achieving a healing rate of 54.5%. On day 10, the wound area had visibly shrunk in all groups, while the differences among these groups were further emphasized. OHA-CMC/CNP and OHA-CMC/EGF remained similar unclosed wound area percentages of 17.3% and 18.6%, respectively, which were remarkably lower than that of the control (31.8%). OHA-CMC/CNP/EGF undoubtedly had the best performance with a closure percentage of 88.3%. At day 15, the skin defect almost disappeared in OHA-CMC/CNP/EGF group. However, the wound regions were still observed in the control, OHA-CMC, OHA-CMC/CNP, and OHA-CMC/CNP/EGF groups, which were 17.0%, 9.8%, 5.6%, and 4.6% of the original wound areas, respectively. These results suggested that OHA-CMC hydrogel had limited positive effects on diabetic wound healing. Individual incorporation of curcumin and EGF into OHA-CMC hydrogel and their sustained release significantly accelerated wound healing. OHA-CMC/CNP/EGF exhibited the best therapeutic efficacy due to the synergistic effects of curcumin and EGF and the elaborate regulation of drug release in a way coordinated with wound healing process by OHA-CMC hydrogel.

Animals from each group were sacrificed on days 5, 10, and 15 to collect wound tissues for histological analysis using H&E staining. The overall histological morphology of the wound bed was observed to examine epidermis and granulation tissue regeneration since re-epithelialization and granulation tissue formation have been recognized as the hallmarks of wound healing [54]. At day 10, the granulation tissues of the control and OHA-CMC groups were loose and incomplete as shown in Fig. 6D. OHA-CMC/CNP and OHA-CMC/EGF treatment resulted in the regeneration of more abundant granulation tissue compared to the control and OHA-CMC groups. The formation of

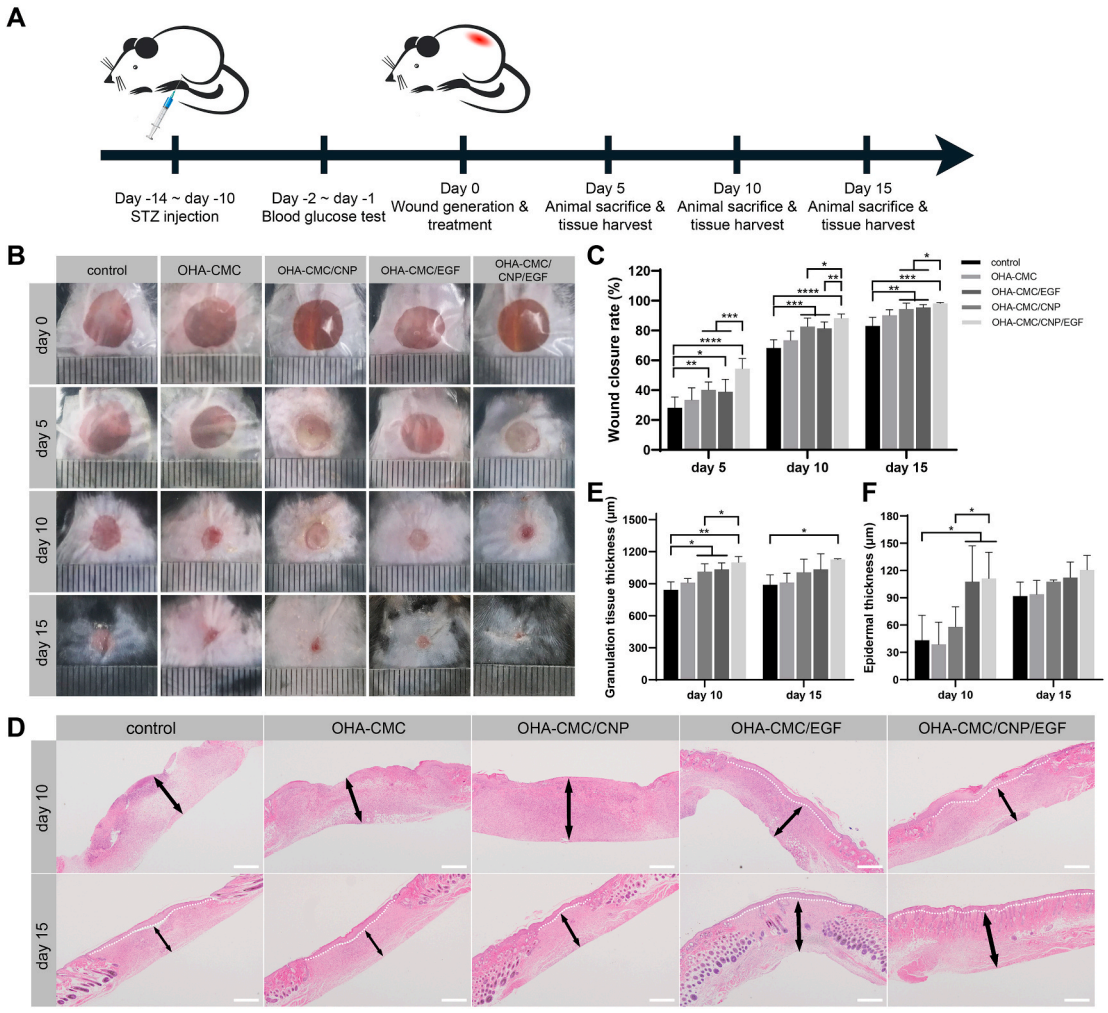

Fig. 6. OHA-CMC/CNP/EGF hydrogel promoted wound healing in STZ-induced diabetic mice. (A) Schematic illustration of the operations on the mouse in an order of time. (B) Representative photographs of the diabetic wound at day 0, 5, 10, and 15 treated with control, OHA-CMC, OHA-CMC/CNP, OHA-CMC/EGF, and OHA-CMC/CNP/EGF groups. (C) Wound closure percentage at day 5, 10, and 15 after treatment with the five groups. (D) H&E staining images indicating the regenerated granulation tissue and epidermis in the wound region following different treatments for 10 and 15 days (white dashed line denotes the boundary of epidermis and dermis; black arrow denotes the granulation tissue). Scale bar: 500 μm. (E) Quantification of granulation tissue thickness following different treatments for 10 and 15 days. (F) Quantification of epidermal thickness following different treatments for 10 and 15 days.

compact and multilayered granulation tissue was observed in the wound treated with OHA-CMC/CNP/EGF, which was thicker than that of any other groups (Fig. 6E). Particularly noteworthy was the exhilarating presence of the intact neoepidermis in wound tissues managed with OHA-CMC/EGF and OHA-CMC/CNP/EGF hydrogels, which was not observed in three other groups (Fig. 6D). This could be attributed to the extraordinary ability of EGF to facilitate cell migration for epidermal regeneration. At day 15, OHA-CMC/CNP/EGF showed the best regenerative efficacy with an increase of 26.8%, 23.7%, 11.9%, and 9.1% in granulation tissue thickness compared to the control, blank hydrogel, CNP- and EGF-loaded hydrogel groups, respectively (Fig. 6E). Neoepidermis was formed in all the treated groups at day 15, while treatment of OHA-CMC/CNP/EGF generated the thickest epidermis of 120.7 μm (Fig. 6D, F). Taken together, the OHA-CMC/CNP/EGF hydrogel exerted integrated therapeutic effects of curcumin and EGF through sequential and sustained release of payloads, leading to the optimal result in granulation tissue formation and re-epithelialization.

The regenerated wound tissues were further examined for inflammation infiltration and the formation of skin appendages to provide a comprehensive histological assessment of wound healing. Varying degrees of acute inflammation were observed in all groups on day 5 (Fig. 7A), which was attributed to the migration of inflammatory cells, including macrophages and monocytes, to the wound region to restore microenvironment homeostasis. Severe inflammation persisted in the wound sites in the control and OHA-CMC groups, indicating the typical prolonged inflammation phase of diabetic wounds. On the contrary, the wound tissues treated with OHA-CMC/CNP and OHA-CMC/CNP/EGF showed relatively moderate inflammation compared to other groups due to the timely and constant release of curcumin from OHA-CMC hydrogel. Many inflammatory cells still remained in the wound bed of the control group at day 10 but were not found in any of the other groups (Fig. 7A), which suggested that the antibacterial properties of OHA-CMC effectively combated infection and contributed to inflammation alleviation. Neovascularization occurred on day 10 in all groups, and formation of more blood vessels was observed in OHA-CMC/CNP, OHA-CMC/EGF, and OHA-CMC/CNP/EGF groups with relative blood vessel amounts of 216%, 227%, and 233%, respectively (Fig. 7A, C). Neovascularization was further improved on day 15, but limited numbers of blood vessels were observed in the control group. Abundant blood vessels were formed in the groups treated with OHA-CMC/CNP, OHA-CMC/EGF, and OHA-CMC/CNP/EGF to support the transport of oxygen and nutrients and the regeneration of skin appendages. As a result, treatment with CNP- and EGF-loaded hydrogels induced the formation of a significantly higher amount of new hair follicles compared with the

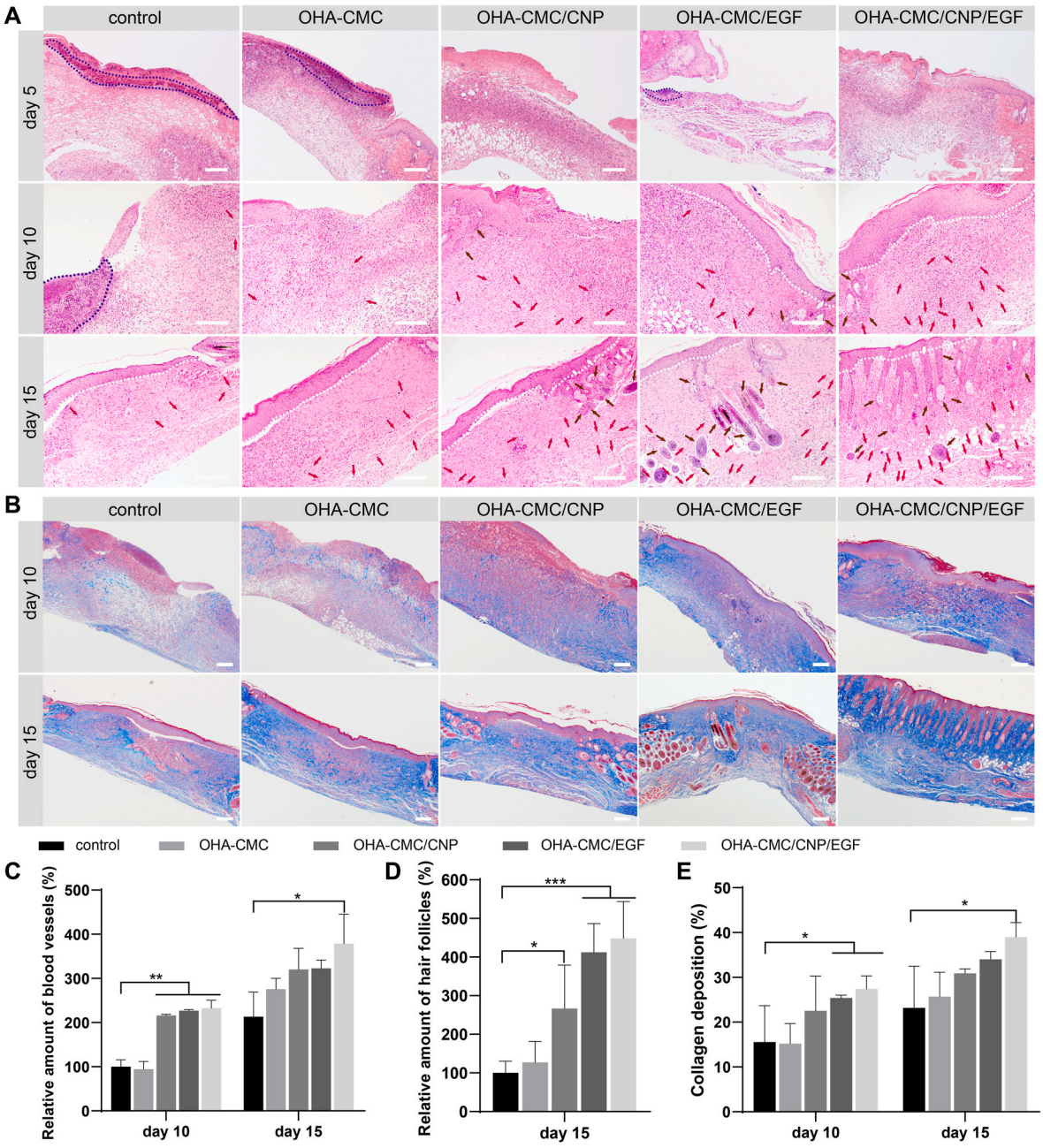

Fig. 7. The effects of the hydrogels on diabetic wound healing evaluated on the histological level. (A) H&E staining images of the wound tissues treated with control, OHA-CMC, OHA-CMC/CNP, OHA-CMC/EGF, and OHA-CMC/CNP/EGF for 5, 10, and 15 days (blue dashed line denotes the inflammatory area; red arrow denotes the blood vessel; brown arrow denotes the hair follicle; white dashed line denotes the boundary of epidermis and dermis). Scale bar: 200 μm. (B) Masson's trichrome staining images of the wound tissues following different treatments for 10 and 15 days. Scale bar: 100 μm. (C) Quantitative analysis of regenerated blood vessels following different treatments for 10 and 15 days. The data was normalized against the control group at day 10 which was defined as 100%. (D) Quantification of regenerated hair follicles following different treatments for 15 days. The data was normalized against the control group which was defined as 100%. (E) Collagen deposition levels in the wound tissues following different treatments for 10 and 15 days. (For interpretation of the references to colour in this figure legend, the reader is referred to the Web version of this article.)

control (Fig. 7A, D). Notably, a considerable amount of hair follicles was generated and regularly arranged under neoepidermis in the OHA-CMC/CNP/EGF group, indicating that skin was nearly completely regenerated following a 15-day treatment of OHA-CMC/CNP/EGF. To sum up, OHA-CMC/CNP/EGF remarkably accelerated diabetic wound healing, which was reflected as the attenuated inflammation infiltration, enhanced re-epithelialization and granulation tissue formation, and reinforced vascularization and skin appendage regeneration.

3.7. Mechanism of hydrogel-mediated beneficial effects on wound healing

To understand the underlying mechanisms through which hydrogels significantly improved diabetic wound healing, key biomarkers and molecules in the wound bed were stained and analyzed. The ROS level of the wound bed was evaluated by DHE staining. OHA-CMC/CNP and OHA-CMC/CNP/EGF significantly reduced ROS production compared to the other groups following the treatments for 5 and 10 days (Fig. 8A, D). It was noteworthy that CNP-loaded hydrogels possessed an excellent ability to persistently attenuate intracellular oxidative stress due to the

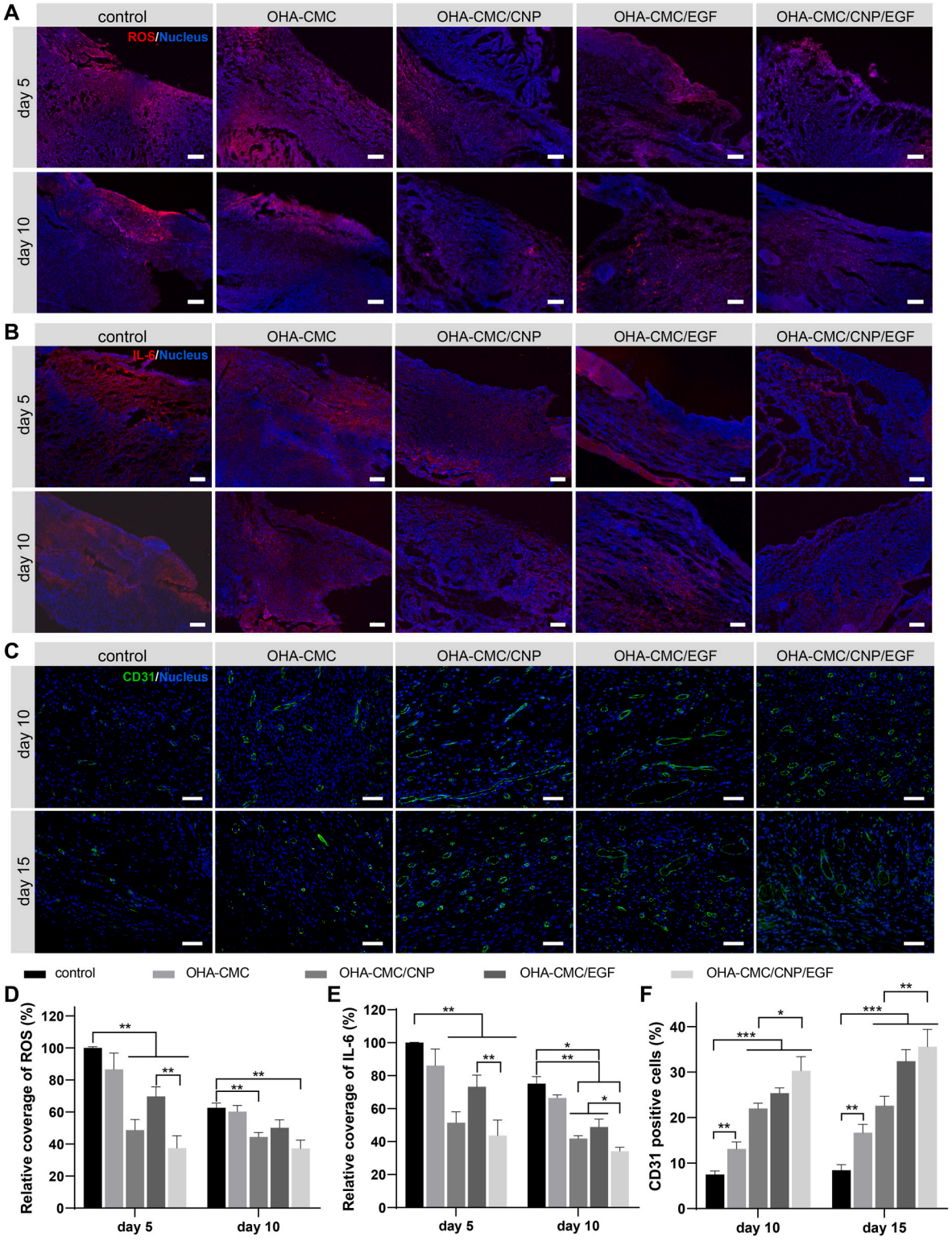

Fig. 8. Mechanism examination of hydrogel-mediated acceleration in wound healing. (A) ROS level of the wound regions indicated by DHE staining following different treatments for 5 and 10 days. Scale bar: 100 μm. (B) Immunofluorescent staining of IL-6 performed on wound tissues from different groups after treating for 5 and 10 days. Scale bar: 200 μm. (C) Neovascularization evaluation through CD31 immunofluorescent staining for the wound tissues treated with different groups for 10 and 15 days. Scale bar: 50 μm. (D, E) Quantitative analysis of ROS (D) and IL-6 (E) labeled structures. The data was normalized against the control group at day 5 which was set as 100%. (F) Quantification of the percentage of CD31 positive cells following the treatments with different groups for 10 and 15 days.

potent antioxidant properties of active curcumin and hydrogel-mediated timely and sustained release. IL-6, a typical pro-inflammatory cytokine regulated by infection and ROS, was evaluated as an indicator of tissue inflammatory responses. As shown in Fig. 8B and E, massive expression of IL-6 was observed in the control group on day 5, which was down-regulated to some extent following treatment with the blank OHA-CMC hydrogel due to its inherent antibacterial activity as evidenced by the above studies (Fig. 3D and E). Treatments with OHA-CMC/CNP

and OHA-CMC/CNP/EGF led to a marked reduction in the red fluorescence intensity by 48.5% and 56.4% compared with the control group, respectively (Fig. 8B, E). These remarkable effects were driven by hydrogel-mediated early release of curcumin concurrent with the inflammation phase of wound healing, and the potent ability of curcumin to suppress inflammation. OHA-CMC/EGF had less inhibitory effects on inflammation due to the delayed release of EGF from the hydrogel, though EGF was reported to induce inflammatory cells to migrate away from the wound bed [55]. All groups presented a decreased IL-6 level after treating for 10 days, while the pattern of expression levels among different groups remained the same as on day 5. These results suggested that early alleviation of inflammation by OHA-CMC/CNP/EGF was beneficial in reducing the typical stalled inflammation phase of diabetic wounds.

Curcumin has well-known anti-inflammatory effects by inhibiting the NF-κB signaling cascade, leading to the downregulation of MMP9, a protease that causes excessive ECM degradation [50]. In this study, the depletion of MMP9 expression was evident following the 5-day treatment with OHA-CMC/CNP and OHA-CMC/CNP/EGF, which showed a 2.45-fold and 3.22-fold decrease in the MMP9 levels compared to that of the control, respectively (Fig. S5A, B). The inhibition of MMP9 expression in the wound bed by CNP-loaded hydrogels was maintained 10 days posttreatment, which was promising to protect the newly formed ECM from undesired degradation. Type I collagen (Col I) is an essential component of dermal ECM and positively affects diabetic wound healing. The presence of Col I was remarkably elevated following the treatments with OHA-CMC/CNP and OHA-CMC/EGF for 10 and 15 days compared with that of control (Fig. S5C, D). OHA-CMC/CNP/EGF treatment resulted in the highest expression level of Col I among the tested groups, which could be attributed to the combinatorial effects of curcumin and EGF that were released at different healing phases. The overall content of collagen in the wound bed was evaluated by Masson's trichrome staining (Fig. 7B, E). Consistent with the Col I immunohistochemistry results, ample and well-organized collagen fibers were observed in OHA-CMC/CNP/EGF treated groups with the highest level of collagen deposition among all groups, which was favorable for improving wound healing and tissue tensile strength.

Neovascularization is considered as one of the key events of diabetic wound healing, as tissue regeneration relies on the oxygen and nutrients transported by blood vessels. The marker of neovascularization, CD31, was therefore stained and analyzed. Extremely limited numbers of blood vessel structures were observed in the control group at day 10 and 15 (Fig. 8C, F). Although treatment with blank OHA-CMC hydrogel led to enhanced CD31 signals, more comprehensive and complete neovascularization with clear lumen structures was observed following the treatment with OHA-CMC/CNP, OHA-CMC/EGF, and OHA-CMC/CNP/EGF, among which the OHA-CMC/CNP/EGF group showed the highest level of neovascularization. The improved angiogenesis and vasculogenesis mediated by OHA-CMC/CNP/EGF ensured skin tissue regeneration during diabetic wound healing, leading to beneficial therapeutic effects.

4. Conclusion

Overall, a novel OHA-CMC hydrogel with sequential release of curcumin and EGF that synchronized with diabetic wound healing process was fabricated in this study. The OHA-CMC hydrogel was identified with superior rheological properties, swelling and degradation kinetics, and biocompatibility, with special emphasis on its inherent potent antibacterial and hemostatic activities. The co-encapsulation of CNP and EGF in OHA-CMC resulted in the rapid and constant release of curcumin to inhibit inflammation and oxidative stress in early phases of wound healing, and the relatively slower and sustained release of EGF to support proliferation and ECM formation in later phases. In vitro results showed that OHA-CMC/CNP/EGF significantly attenuated intracellular oxidative stress and inflammation, and promoted cell migration. In a full-thickness skin defect model of the diabetic mouse, OHA-CMC/CNP/EGF contributed to the fastest wound closure with ideal re-epithelialization, granulation tissue formation, and regeneration of blood vessels and hair follicles. Further mechanism studies revealed that OHA-CMC/CNP/EGF relieved oxidative stress, downregulated the expression of inflammatory cytokines and downstream MMP9, promoted collagen deposition, and accelerated angiogenesis, thus having dramatic therapeutic effects on diabetic wounds. In conclusion, our rational design combining beneficial inherent antibacterial and hemostatic activities and sequential release of curcumin and EGF presents a promising hydrogel material approach to promote diabetic wound healing.

CRediT authorship contribution statement

Bin Hu: Investigation, Methodology, Data curation, Writing – original draft. **Mingzhu Gao:** Investigation, Methodology. **Kofi Oti Boakye-Yiadom:** Writing – review & editing. **William Ho:** Writing – review & editing. **Wei Yu:** Methodology. **Xiaoyang Xu:** Methodology, Supervision, Writing – review & editing. **Xue-Qing Zhang:** Conceptualization, Supervision, Funding acquisition, Writing – review & editing.

Declaration of competing interest

The authors declare that they have no known competing financial interests or personal relationships that could have appeared to influence the work reported in this paper.

Acknowledgment

X. Zhang acknowledges the financial support from the Interdisciplinary Program of Shanghai Jiao Tong University (project number ZH2018ZDA36 (19X190020006)), Shanghai Jiao Tong University Scientific and Technological Innovation Funds (2019TPA10), and the Foundation of National Facility for Translational Medicine (Shanghai) (TMSK-2020-008).

Appendix A. Supplementary data

Supplementary data to this article can be found online at https://doi.org/10.1016/j.bioactmat.2021.04.040.

References

[1] D.G. Armstrong, A.J.M. Boulton, S.A. Bus, Diabetic foot ulcers and their recurrence, N. Engl. J. Med. 376 (24) (2017) 2367–2375, https://doi.org/10.1056/NEJMra1615439.
[2] P.R. Cavanagh, B.A. Lipsky, A.W. Bradbury, G. Botek, Treatment for diabetic foot ulcers, Lancet 366 (9498) (2005) 1725–1735, https://doi.org/10.1016/s0140-6736(05)67699-4.
[3] D. Stern, H. Cui, Crafting polymeric and peptidic hydrogels for improved wound healing, Adv. Healthc. Mater. 8 (9) (2019), https://doi.org/10.1002/adhm.201900104.
[4] L.I.F. Moura, A.M.A. Dias, E. Carvalho, H.C. de Sousa, Recent advances on the development of wound dressings for diabetic foot ulcer treatment-A review, Acta Biomater. 9 (7) (2013) 7093–7114, https://doi.org/10.1016/j.actbio.2013.03.033.
[5] Y.-I. Shen, H. Cho, A.E. Papa, J.A. Burke, X.Y. Chan, E.J. Duh, S. Gerecht, Engineered human vascularized constructs accelerate diabetic wound healing, Biomaterials 102 (2016) 107–119, https://doi.org/10.1016/j.biomaterials.2016.06.009.
[6] H. Cho, M.R. Blatchley, E.J. Duh, S. Gerecht, Acellular and cellular approaches to improve diabetic wound healing, Adv. Drug Deliv. Rev. 146 (2019) 267–288, https://doi.org/10.1016/j.addr.2018.07.019.
[7] R.E. Mirza, M.M. Fang, W.J. Ennis, T.J. Koh, Blocking interleukin-1 beta induces a healing-associated wound macrophage phenotype and improves healing in type 2 diabetes, Diabetes 62 (7) (2013) 2579–2587, https://doi.org/10.2337/db12-1450.
[8] S.L. Wong, M. Demers, K. Martinod, M. Gallant, Y. Wang, A.B. Goldfine, C.R. Kahn, D.D. Wagner, Diabetes primes neutrophils to undergo NETosis, which impairs wound healing, Nat. Med. 21 (7) (2015) 815, https://doi.org/10.1038/nm.3887.
[9] T. Shen, K. Dai, Y. Yu, J. Wang, C. Liu, Sulfated chitosan rescues dysfunctional macrophages and accelerates wound healing in diabetic mice, Acta Biomater. 117 (2020) 192–203, https://doi.org/10.1016/j.actbio.2020.09.035.

[10] Y. Xiao, L.A. Reis, N. Feric, E.J. Knee, J. Gu, S. Cao, C. Laschinger, C. Londono, J. Antolovich, A.P. McGuigan, M. Radisic, Diabetic wound regeneration using peptide-modified hydrogels to target re-epithelialization, Proc. Natl. Acad. Sci. U. S. A 113 (40) (2016) E5792–E5801, https://doi.org/10.1073/pnas.1612277113.

[11] B. Kunkemoeller, T.R. Kyriakides, Redox signaling in diabetic wound healing regulates extracellular matrix deposition, Antioxidants Redox Signal. 27 (12) (2017) 823–838, https://doi.org/10.1089/ars.2017.7263.

[12] B. Joe, M. Vijaykumar, B.R. Lokesh, Biological properties of curcumin-cellular and molecular mechanisms of action, Crit. Rev. Food Sci. Nutr. 44 (2) (2004) 97–111, https://doi.org/10.1080/10408690490424702.

[13] D. Akbik, M. Ghadiri, W. Chrzanowski, R. Rohanizadeh, Curcumin as a wound healing agent, Life Sci. 116 (1) (2014) 1–7, https://doi.org/10.1016/j.lfs.2014.08.016.

[14] Z. Hussain, H.E. Thu, S.-F. Ng, S. Khan, H. Katas, Nanoencapsulation, an efficient and promising approach to maximize wound healing efficacy of curcumin: a review of new trends and state-of-the-art, Colloids Surf. B Biointerfaces 150 (2017) 223–241, https://doi.org/10.1016/j.colsurfb.2016.11.036.

[15] N.E. Rainey, A. Moustapha, P.X. Petit, Curcumin, a multifaceted hormetic agent, mediates an intricate crosstalk between mitochondrial turnover, autophagy, and apoptosis. Oxidative Medicine and Cellular Longevity 2020, 2020, https://doi.org/10.1155/2020/3656419.

[16] J. Hardwicke, D. Schmaljohann, D. Boyce, D. Thomas, Epidermal growth factor therapy and wound healing - past, present and future, Surgeon-J. Royal Colleges Surg. Edinburgh Ireland 6 (3) (2008) 172–177, https://doi.org/10.1016/s1479-666x(08)80114-x.

[17] U. Freudenberg, A. Zieris, K. Chwalek, M.V. Tsurkan, M.F. Maitz, P. Atallah, K. R. Levental, S.A. Eming, C. Werner, Heparin desulfation modulates VEGF release and angiogenesis in diabetic wounds, J. Contr. Release 220 (2015) 79–88, https://doi.org/10.1016/j.jconrel.2015.10.028.

[18] K. Ulubayram, A.N. Cakar, P. Korkusuz, C. Ertan, N. Hasirci, EGF containing gelatin-based wound dressings, Biomaterials 22 (11) (2001) 1345–1356, https://doi.org/10.1016/s0142-9612(00)00287-8.

[19] N. Zandi, B. Dolatyar, R. Lotfi, Y. Shallageh, M.A. Shokrgozar, E. Tamjid, N. Annabi, A. Simchi, Biomimetic nanoengineered scaffold for enhanced full-thickness cutaneous wound healing, Acta Biomater. 124 (2021) 191–204, https://doi.org/10.1016/j.actbio.2021.01.029.

[20] W. Zhao, Y. Li, X. Zhang, R. Zhang, Y. Hu, C. Boyer, F.-J. Xu, Photo -responsive supramolecular hyaluronic acid hydrogels for accelerated wound healing, J. Contr. Release 323 (2020) 24–35, https://doi.org/10.1016/j.jconrel.2020.04.014.

[21] R. Augustine, A. Hasan, Y.B. Dalvi, S.R.U. Rehman, R. Varghese, R.N. Unni, H. C. Yalcin, R. Alfkey, S. Thomas, A.-E. Al Moustafa, Growth factor loaded in situ photocrosslinkable poly(3-hydroxybutyrate-co-3-hydroxyvalerate)/gelatin methacryloyl hybrid patch for diabetic wound healing, Mater. Sci. Eng. C-Mater. Biol. Appl. 118 (2021), https://doi.org/10.1016/j.msec.2020.111519.

[22] X. Li, X. Ye, J. Qi, R. Fan, X. Gao, Y. Wu, L. Zhou, A. Tong, G. Guo, EGF and curcumin co-encapsulated nanoparticle/hydrogel system as potent skin regeneration agent, Int. J. Nanomed. 11 (2016) 3993–4009, https://doi.org/10.2147/ijn.S104350.

[23] C. Mohanty, J. Pradhan, A human epidermal growth factor-curcumin bandage bioconjugate loaded with mesenchymal stem cell for in vivo diabetic wound healing, Mater. Sci. Eng. C-Mater. Biol. Appl. 111 (2020), https://doi.org/10.1016/j.msec.2020.110751.

[24] H.-J. Lee, M. Jeong, Y.-G. Na, S.-J. Kim, H.-K. Lee, C.-W. Cho, An EGF- and curcumin-Co-encapsulated nanostructured lipid carrier accelerates chronic-wound healing in diabetic rats, Molecules 25 (20) (2020), https://doi.org/10.3390/molecules25204610.

[25] C. Xu, W. Lee, G. Dai, Y. Hong, Highly elastic biodegradable single-network hydrogel for cell printing, ACS Appl. Mater. Interfaces 10 (12) (2018) 9969–9979, https://doi.org/10.1021/acsami.8b01294.

[26] G. Chen, Y. Yu, X. Wu, G. Wang, J. Ren, Y. Zhao, Bioinspired multifunctional hybrid hydrogel promotes wound healing, Adv. Funct. Mater. 28 (33) (2018), https://doi.org/10.1002/adfm.201801386.

[27] Y.S. Zhang, A. Khademhosseini, Advances in engineering hydrogels, Science 356 (6337) (2017) 10, https://doi.org/10.1126/science.aaf3627.

[28] H. Ruan, Q. Hu, D. Wen, Q. Chen, G. Chen, Y. Lu, J. Wang, H. Cheng, W. Lu, Z. Gu, A dual-bioresponsive drug-delivery depot for combination of epigenetic modulation and immune checkpoint blockade, Adv. Mater. 31 (17) (2019), https://doi.org/10.1002/adma.201806957.

[29] J. Xu, Q. Feng, S. Lin, W. Yuan, R. Li, J. Li, K. Wei, X. Chen, K. Zhang, Y. Yang, T. Wu, B. Wang, M. Zhu, R. Guo, G. Li, L. Bian, Injectable stem cell-laden supramolecular hydrogels enhance in situ osteochondral regeneration via the sustained co-delivery of hydrophilic and hydrophobic chondrogenic molecules, Biomaterials 210 (2019) 51–61, https://doi.org/10.1016/j.biomaterials.2019.04.031.

[30] C. Hong, D. Song, D.-K. Lee, L. Lin, H.C. Pan, D. Lee, P. Deng, Z. Liu, D. Hadaya, H.-L. Lee, A. Mohammad, X. Zhang, M. Lee, C.-Y. Wang, D. Ho, Reducing posttreatment relapse in cleft lip palatal expansion using an injectable estrogen-nanodiamond hydrogel, Proc. Natl. Acad. Sci. U. S. A 114 (35) (2017) E7218–E7225, https://doi.org/10.1073/pnas.1704027114.

[31] B. Khorsand, T.M. Acri, D. Anh-Vu, J.E. Femino, E. Petersen, D.C. Fredericks, A. K. Salem, A multi-functional implant induces bone formation in a diabetic model, Adv. Healthc. Mater. 9 (18) (2020), https://doi.org/10.1002/adhm.202000770.

[32] S. Yan, Q. Zhang, J. Wang, Y. Liu, S. Lu, M. Li, D.L. Kaplan, Silk fibroin/chondroitin sulfate/hyaluronic acid ternary scaffolds for dermal tissue reconstruction, Acta Biomater. 9 (6) (2013) 6771–6782, https://doi.org/10.1016/j.actbio.2013.02.016.

[33] Y. Liang, X. Zhao, T. Hu, B. Chen, Z. Yin, P.X. Ma, B. Guo, Adhesive hemostatic conducting injectable composite hydrogels with sustained drug release and photothermal antibacterial activity to promote full-thickness skin regeneration during wound healing, Small 15 (12) (2019), https://doi.org/10.1002/smll.201900046.

[34] A. Moeini, P. Pedram, P. Makvandi, M. Malinconico, G.G. d'Ayala, Wound healing and antimicrobial effect of active secondary metabolites in chitosan-based wound dressings: a review, Carbohydr. Polym. 233 (2020), https://doi.org/10.1016/j.carbpol.2020.115839.

[35] H. Tan, C.R. Chu, K.A. Payne, K.G. Marra, Injectable in situ forming biodegradable chitosan-hyaluronic acid based hydrogels for cartilage tissue engineering, Biomaterials 30 (13) (2009) 2499–2506, https://doi.org/10.1016/j.biomaterials.2008.12.080.

[36] S. Yan, T. Wang, L. Feng, J. Zhu, K. Zhang, X. Chen, L. Cui, J. Yin, Injectable in situ self-cross-linking hydrogels based on poly(L-glutamic acid) and alginate for cartilage tissue engineering, Biomacromolecules 15 (12) (2014) 4495–4508, https://doi.org/10.1021/bm501313t.

[37] W. Huang, Y. Wang, Z. Huang, X. Wang, L. Chen, Y. Zhang, L. Zhang, On-demand dissolvable self-healing hydrogel based on carboxymethyl chitosan and cellulose nanocrystal for deep partial thickness burn wound healing, ACS Appl. Mater. Interfaces 10 (48) (2018) 41076–41088, https://doi.org/10.1021/acsami.8b14526.

[38] J. Qu, X. Zhao, Y. Liang, Y. Xu, P.X. Ma, B. Guo, Degradable conductive injectable hydrogels as novel antibacterial, anti-oxidant wound dressings for wound healing, Chem. Eng. J. 362 (2019) 548–560, https://doi.org/10.1016/j.cej.2019.01.028.

[39] F. Sun, Y. Bu, Y. Chen, F. Yang, J. Yu, D. Wu, An injectable and instant self-healing medical adhesive for wound sealing, ACS Appl. Mater. Interfaces 12 (8) (2020) 9132–9140, https://doi.org/10.1021/acsami.0c01022.

[40] Y.-H. Tsou, X.-Q. Zhang, X. Bai, H. Zhu, Z. Li, Y. Liu, J. Shi, X. Xu, Dopant-free hydrogels with intrinsic photoluminescence and biodegradable properties, Adv. Funct. Mater. 28 (34) (2018), https://doi.org/10.1002/adfm.201802607.

[41] N. Artzi, N. Oliva, C. Puron, S. Shitreet, S. Artzi, A.B. Ramos, A. Groothuis, G. Sahagian, E.R. Edelman, In vivo and in vitro tracking of erosion in biodegradable materials using non-invasive fluorescence imaging, Nat. Mater. 10 (9) (2011) 704–709, https://doi.org/10.1038/nmat3095.

[42] B. Song, E. Zhang, X. Han, H. Zhu, Y. Shi, Z. Cao, Engineering and application perspectives on designing an antimicrobial surface, ACS Appl. Mater. Interfaces 12 (19) (2020) 21330–21341, https://doi.org/10.1021/acsami.9b19992.

[43] G. Geisberger, E.B. Gyenge, D. Hinger, A. Kaech, C. Maake, G.R. Patzke, Chitosan-thioglycolic acid as a versatile antimicrobial agent, Biomacromolecules 14 (4) (2013) 1010–1017, https://doi.org/10.1021/bm3018593.

[44] S. Wang, H. Zheng, L. Zhou, F. Cheng, Z. Liu, H. Zhang, L. Wang, Q. Zhang, Nanoenzyme-reinforced injectable hydrogel for healing diabetic wounds infected with multidrug resistant bacteria, Nano Lett. 20 (7) (2020) 5149–5158, https://doi.org/10.1021/acs.nanolett.0c01371.

[45] M. Wang, C. Wang, M. Chen, Y. Xi, W. Cheng, C. Mao, T. Xu, X. Zhang, C. Lin, W. Gao, Y. Guo, B. Lei, Efficient angiogenesis-based diabetic wound healing/skin reconstruction through bioactive antibacterial adhesive ultraviolet shielding nanodressing with exosome release, ACS Nano 13 (9) (2019) 10279–10293, https://doi.org/10.1021/acsnano.9b03656.

[46] J. Liu, Z. Chen, J. Wang, R. Li, T. Li, M. Chang, F. Yan, Y. Wang, Encapsulation of curcumin nanoparticles with MMP9-responsive and thermos-sensitive hydrogel improves diabetic wound healing, ACS Appl. Mater. Interfaces 10 (19) (2018) 16315–16326, https://doi.org/10.1021/acsami.8b03868.

[47] Y. Zhu, Z. Cankova, M. Iwanaszko, S. Lichtor, M. Mrksich, G.A. Ameer, Potent laminin-inspired antioxidant regenerative dressing accelerates wound healing in diabetes, Proc. Natl. Acad. Sci. U. S. A 115 (26) (2018) 6816–6821, https://doi.org/10.1073/pnas.1804262115.

[48] J. Ancerewicz, E. Migliavacca, P.A. Carrupt, B. Testa, F. Bree, R. Zini, J. P. Tillement, S. Labidalle, D. Guyot, A.M. Chauvet-Monges, A. Crevat, A. Le Ridant, Structure-property relationships of trimetazidine derivatives and model compounds as potential antioxidants, Free Radic. Biol. Med. 25 (1) (1998) 113–120, https://doi.org/10.1016/s0891-5849(98)00072-0.

[49] Y. Wu, Y. Quan, Y. Liu, K. Liu, H. Li, Z. Jiang, T. Zhang, H. Lei, K.A. Radek, D. Li, Z. Wang, J. Lu, W. Wang, S. Ji, Z. Xia, Y. Lai, Hyperglycaemia inhibits REG3A expression to exacerbate TLR3-mediated skin inflammation in diabetes, Nat. Commun. 7 (2016), https://doi.org/10.1038/ncomms13393.

[50] Y. Wang, T. Ying, J. Li, Y. Xu, R. Wang, Q. Ke, S.G.F. Shen, H. Xu, K. Lin, Hierarchical micro/nanofibrous scaffolds incorporated with curcumin and zinc ion eutectic metal organic frameworks for enhanced diabetic wound healing via anti-oxidant and anti-inflammatory activities, Chem. Eng. J. 402 (2020), https://doi.org/10.1016/j.cej.2020.126273.

[51] X. Alvarez, A. Alves, M.P. Ribeiro, M. Lazzari, P. Coutinho, A. Otero, Biochemical characterization of Nostoc sp. exopolysaccharides and evaluation of potential use in wound healing, Carbohydr. Polym. 254 (2021), https://doi.org/10.1016/j.carbpol.2020.117303.

[52] N.R. Johnson, Y. Wang, Controlled delivery of heparin-binding EGF-like growth factor yields fast and comprehensive wound healing, J. Contr. Release 166 (2) (2013) 124–129, https://doi.org/10.1016/j.jconrel.2012.11.004.

[53] X. Wang, J. Ge, E.E. Tredget, Y. Wu, The mouse excisional wound splinting model, including applications for stem cell transplantation, Nat. Protoc. 8 (2) (2013) 302–309, https://doi.org/10.1038/nprot.2013.002.
[54] P. Rousselle, F. Braye, G. Dayan, Re-epithelialization of adult skin wounds: cellular mechanisms and therapeutic strategies, Adv. Drug Deliv. Rev. 146 (2019) 344–365, https://doi.org/10.1016/j.addr.2018.06.019.
[55] J. Zhang, W. Hu, Q. Diao, Z. Wang, J. Miao, X. Chen, Z. Xue, Therapeutic effect of the epidermal growth factor on diabetic foot ulcer and the underlying mechanisms, Exp. Therapeut. Med. 17 (3) (2019) 1643–1648, https://doi.org/10.3892/etm.2018.7133.